

# Radio Morphing: Fast computation of inclined air shower radio emission

Simon Chiche<sup>a</sup>, Olivier Martineau-Huynh<sup>b,a</sup>, Matias Tueros<sup>c,d,a</sup>, Krijn D. de Vries<sup>e</sup>

<sup>a</sup>*Sorbonne Université, CNRS, UMR 7095, Institut d’Astrophysique de Paris, 98 bis bd Arago, 75014 Paris, France*

<sup>b</sup>*Sorbonne Université, Université Paris Diderot, Sorbonne Paris Cité, CNRS, Laboratoire de Physique Nucléaire et de Hautes Energies (LPNHE), Paris, France*

<sup>c</sup>*IFLP - CCT La Plata - CONICET, Casilla de Correo 727 (1900) La Plata, Argentina*

<sup>d</sup>*Dep. de Fisica, Fac. de Cs. Ex., Universidad Nacional de La Plata, Casilla de Correo 67 (1900) La Plata, Argentina*

<sup>e</sup>*Vrije Universiteit Brussel, Physics Department, Pleinlaan 2, 1050 Brussels, Belgium*

---

## Abstract

The preparation of next-generation large-scale radio experiments requires running a fast and efficient number of simulations to explore multiple detector configurations over vast areas and develop novel methods for the reconstruction of air shower parameters. While Monte Carlo simulations are accurate and reliable tools, they are too computationally expensive to explore the full parameter space of these new detectors within a reasonable timescale. We introduce a new version of Radio Morphing, a semi-analytical tool designed to simulate the radio emission of any cosmic-ray induced air shower with zenith angle  $\theta > 60^\circ$ , at any desired antenna position, from the simulation data of a few reference showers at given positions. We present the latest performances of Radio Morphing which now provides simulation of air shower radio signals with average relative differences on the peak amplitude below 17% on raw traces, below 15% with a  $3\sigma$  trigger threshold, below 13% in the [50 – 200] MHz band, and even below  $\sim 10\%$  in the [30 – 80] MHz band. These results are combined with a computation time reduced by more than four orders of magnitude, compared to standard Monte Carlo simulations.

**Keywords:** Radio-detection, High-energy astroparticles, Air-shower simulations

---

## 1. Introduction

Radio detection is now a mature, well-established technique, used by a wide range of experiments for air shower detection to unveil the high-energy Universe. Large-scale radio experiments such as GRAND [1], BEACON [2], SKA [3], or the radio upgrade of the Pierre Auger Observatory [4] are now being built to reach unprecedented sensitivity, field of view, and angular resolution at the highest energies. This goal requires to run a large number of air-shower simulations to explore different antenna configurations, test reconstruction methods, and evaluate the detector performances. While Monte Carlo simulations such as ZHAireS [5, 6] and Coreas [7, 8] provide accurate simulation results, these are too computationally intensive to explore all the parameter space with large-scale experiments. On the other hand, macroscopic approaches such as MGMR [9, 10] are much faster but limited by our

incomplete knowledge of the physical processes, particularly when looking for showers with very inclined arrival directions. This motivates the need to develop fast and accurate simulations of the radio signal. Already significant efforts have been made towards this direction, with template synthesis for vertical and mildly inclined showers [11]. On the other hand, inclined showers remain challenging because of asymmetry effects and rapid changes in the emission with the shower zenith angle. We introduce here a new version of Radio Morphing, a semi-analytical tool designed to simulate the radio emission from any air shower with zenith angle above  $60^\circ$ , at any position, from the reference data of a few simulated showers at given positions. The current version incorporates shower-to-shower fluctuations, refined scaling laws, interpolation method, and reference library compared to the version of [12]. We present the current Radio Morphing method and its implementation in Sections 2 and 3 respectively, and show the latest Radio Morphing performances in Section 4.

---

*Email address:* `simon.chiche@ulb.be` (Simon Chiche)

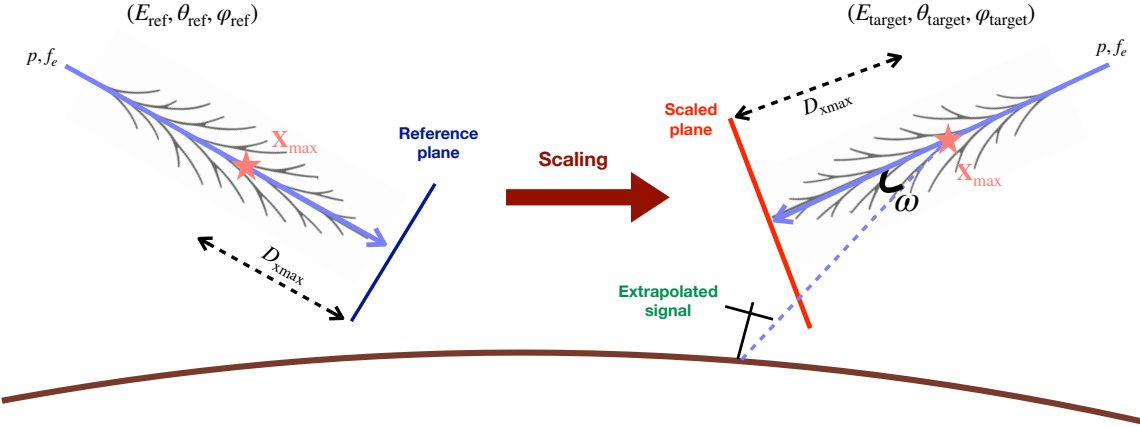


Figure 1: Sketch of the Radio Morphing procedure. The electric field from a reference ZHAireS simulation with parameters  $[E_{\text{ref}}, \theta_{\text{ref}}, \varphi_{\text{ref}}, D_{\text{xmax}}]$  (blue “reference plane”) is scaled towards a shower with  $[E_{\text{target}}, \theta_{\text{target}}, \varphi_{\text{target}}, D_{\text{xmax}}]$  (red “scaled plane”). The resulting signal is then interpolated within the plane and extrapolated along the shower axis to infer the radio-emission at any position.

## 2. The Radio Morphing method

The Radio Morphing method is related to the principle of the universality of air showers, which assumes that the radio emission, supposed point-like, can be fully inferred by characterizing the shower at its maximum development  $X_{\text{max}}$  [13]. Based on this hypothesis, the variations in the radio emission between different showers can directly be modeled by accounting for the variations at  $X_{\text{max}}$ . This assumption is particularly accurate for inclined air showers, for which the distance to the observer is large with respect to the emission region.

### 2.1. First principles of Radio Morphing

The Radio Morphing procedure can be divided into two steps illustrated in Fig. 1:

(1) First, the *scaling* procedure: We select a reference shower, simulated with ZHAireS, from our library (introduced in Section 2.2), for which the electric field was simulated at sampled antenna positions in planes perpendicular to the shower axis located at various distances from  $X_{\text{max}}$ , as illustrated by the blue “reference” plane in Fig. 1. The electric field traces of this shower are then scaled using simple laws based on physical principles to infer the radio emission from a target shower with different primary composition, energy, and arrival direction, at sampled antenna positions located at the same  $X_{\text{max}}$  distance  $D_{\text{xmax}}$  and aperture angle  $\omega$  as the reference ones (scaled plane in Fig. 1).

(2) The *interpolation* procedure: we then use the electric field traces at the scaled positions to interpolate the radio signal at any position within the plane. Eventually, we extrapolate the radio emission at any given

position in space along the shower axis, indicated for example by the green “extrapolated” signal.

We mention that the whole Radio Morphing procedure is performed on the full-band electric field traces, to infer general results that can then be filtered in the desired frequency range, similarly to Monte Carlo simulations.

### 2.2. Reference library and plane selection

The Radio Morphing requires first to build a set of reference simulations, that we simulated with ZHAireS and that can be used to scale the radio emission towards the target showers. The initial Radio Morphing implementation was using only one reference shower, but we chose to use multiple showers to reduce the error introduced by the scaling procedure and improve the efficiency of the method. These showers must be chosen wisely to sample the parameter space at limited computing costs. For our reference library, we simulated 16 ZHAireS iron-induced showers. Iron primaries were favored compared to lighter ones, because of their reduced shower-to-shower fluctuations, but these showers can then be used to generate showers for any other cosmic ray primary. All our reference showers were chosen with a primary energy of 3.98 EeV and an azimuth angle  $\varphi = 90^\circ$  (shower propagating towards the East). Since for inclined showers the radio emission changes rapidly with the shower inclination, we considered 16 zenith bins linear in  $1/\log_{10}(\cos \theta)$  to allow for a denser sampling of inclined showers, following:  $\theta = [65.5^\circ, 67.8^\circ, 69.8^\circ, 74.8^\circ, 76.1^\circ, 77.4^\circ, 78.5^\circ, 79.5^\circ]$ ,

$80.4^\circ, 82.7^\circ, 83.4^\circ, 84.5^\circ, 85.0^\circ, 86.2^\circ, 86.5^\circ, 86.8^\circ$ . Computation points were placed in planes perpendicular to the shower axis, at various distances between  $X_{\max}$  and a ground altitude of 1000 meters above sea level. Each plane consists of a star-shape layout with 193 antennas, but the number of planes used typically increases with zenith angle to account for the larger ground- $X_{\max}$  distance at higher inclination, which is another improvement compared to [12]. For all our simulations we used SIBYLL23d as hadronic model, a typical magnetic field of Dunhuang (China) with amplitude  $B = 56 \mu\text{T}$ , and inclination  $i = 60.8^\circ$ , Linsley 5-layers atmospheric model [14] and a relative thinning of  $10^{-5}$ .

When generating a Radio Morphing simulation, the user must specify a target primary energy, zenith and azimuth angle ( $E_t, \theta_t, \varphi_t$ ). We thus chose, in our library, the reference ZHAireS simulation with the closest zenith angle  $\theta_{\text{ref}}$ . The user must also specify a coordinate list of target antenna positions  $(x_t, y_t, z_t)$  in the AIRES reference frame, at which the radio signal will be computed. Hence, for each target antenna, we chose within the selected ZHAireS simulation, the reference plane with  $X_{\max}$  distance  $D_{\text{plane}}$  that is the closest to the  $X_{\max}$ -antenna distance  $d_{\text{ant}}$ . This procedure is done to reduce as much as possible the error related to the extrapolation of the signal.

### 3. Radio Morphing implementation

To morph a reference shower with primary energy, arrival direction and mass number  $(E_r, \varphi_r, \theta_r, A_r)$  into a target shower with  $(E_t, \varphi_t, \theta_t, A_t)$ , we need to account for the variation of the radio emission with the shower parameters. For this, we can rely on scaling laws, mainly based on the physical properties of the shower emission. The current Radio Morphing implementation follows similar principles to the version of [12], but with several refinements to improve its efficiency and range of validity. For completeness, we detail the full scaling procedure and highlight the specific improvements when appropriate.

#### 3.1. Primary composition

For cosmic ray showers, changes in the primary nature mainly affect the radio emission through a modification of the  $X_{\max}$  position, since showers induced by light primaries develop deeper in the atmosphere than those induced by heavy nuclei. In this new version of Radio Morphing, we model these effects by parametrizing the mean  $X_{\max}$  grammage of proton and iron induced

air showers, with  $\sim 11\,000$  ZHAireS simulations, using SYBILL23d as hadronic model, following

$$\langle X_{\max} \rangle = a \log_{10} E[\text{TeV}] + c, \quad (1)$$

with  $E$  being the shower primary energy. We find  $a = 57.4 \text{ g.cm}^{-2}$ ,  $c = 421.9 \text{ g.cm}^{-2}$  for proton-induced showers and  $a = 65.2 \text{ g.cm}^{-2}$ ,  $c = 270.6 \text{ g.cm}^{-2}$  for iron showers. From Eq 3.1, we can then derive the  $X_{\max}$  coordinates of the target shower by numerically integrating the grammage along the shower axis, assuming Linsley's atmospheric model. This  $X_{\max}$  position is then assumed to be the point-like source of the target shower radio emission. We mention that we used here a parametrization of  $\langle X_{\max} \rangle$  based on numerical simulations, instead of an empirical one, in order to get results as close as possible to ZHAireS simulations. The current Radio Morphing implements only proton and iron primaries, but it would be straightforward to implement other cosmic ray primaries using a similar parametrization.

#### 3.2. Energy scaling

In air showers, the number of particles at  $X_{\max}$  is expected to increase linearly with the primary particle energy ([15]). Additionally, for a coherent emission, the radiation energy scales with the squared number of emitters. This implies that at first order, the radio signal electric field amplitude at the antenna level increases linearly with the primary particle energy. Following [12], the scaling of the electric field amplitude  $\mathcal{E}$  between a reference shower with primary energy  $E_r$  and the same target shower but with primary energy  $E_t$  is given by

$$\mathcal{E}^t(t) = \frac{E_t}{E_r} \mathcal{E}^r(t) = k_E \mathcal{E}^r(t), \quad (2)$$

where we introduced  $k_E = E_t/E_r$ . We note here that rigorously, we should scale the electric field traces with the shower electromagnetic energy rather than with the primary energy, as hadrons for example, do not contribute to the radio emission. Yet, the correction is minor, and we assumed that it can be neglected with respect to the other sources of uncertainties in the Radio Morphing method.

We illustrate the scaling procedure in the top plots of Fig. 2, where we show the lateral distribution function (LDF) of the radio signal along the  $(\mathbf{v} \times \mathbf{B})$  direction, for two showers with different energies but the same directions, before (left-hand panel) and after (right-hand

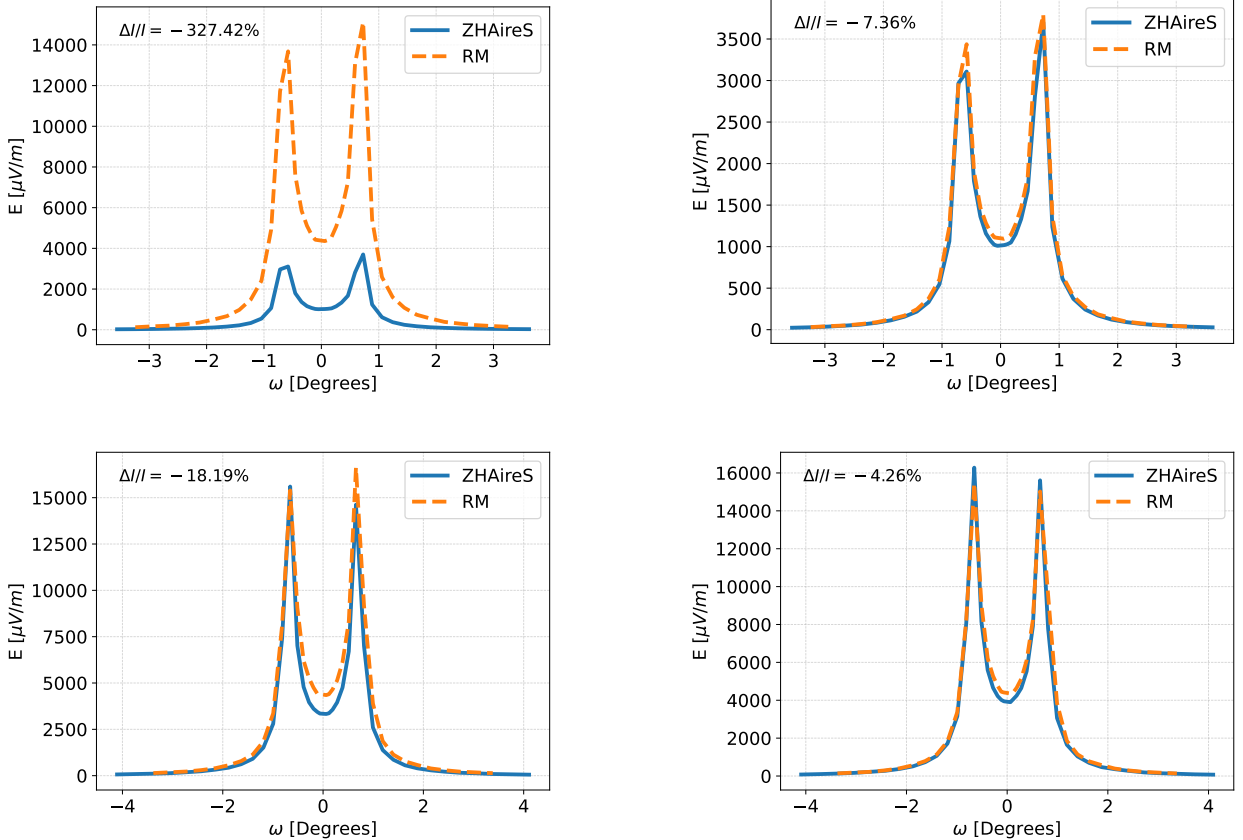


Figure 2: (Top) Lateral distribution functions (LDFs) for two showers with the same arrival directions ( $\theta = 75^\circ$ ,  $\varphi = 90^\circ$ ), but different primary energies ( $E_r = 3.98$  EeV,  $E_t = 1.0$  EeV) without any energy scaling (top left) and with the energy scaling procedure (top right). The  $\omega$  angle corresponds to the angular deviation from the shower axis, taken from  $X_{\max}$  as shown in Fig. 1. (Bottom) LDFs for two showers with the same primary energy and zenith angle ( $E = 3.98$  EeV,  $\theta = 75^\circ$ ), but different azimuth angles ( $\varphi_r = 90^\circ$ ,  $\varphi_t = 0^\circ$ ), with (left) and without (right) applying the scaling procedure.

panel) the scaling. It can be seen that the LDF shows a much better agreement after the scaling procedure is applied. We can quantify the agreement between both showers by computing the relative differences in the integral of their LDFs noted  $I$ . In the case where no scaling is applied, we find  $\delta I/I = (I_{\text{ZHS}} - I_{\text{RM}})/I_{\text{ZHS}} = 327\%$ , while  $\delta I/I = -7\%$  after the scaling procedure.

### 3.3. Geomagnetic angle

A change in the shower direction will have two main effects: a change in the geomagnetic angle  $\alpha = \arccos(\mathbf{u}_v \cdot \mathbf{u}_B)$ , with  $\mathbf{u}_v$  and  $\mathbf{u}_B$  the shower and magnetic field direction respectively, and a change in the altitude at  $X_{\max}$ . The scaling with the geomagnetic angle incorporates all the effects related to the change in the shower azimuth, while the scaling with the altitude, discussed in the next section, is purely related to a primary composition and zenith angle effect.

Two main processes account for the radio emission in air showers, the dominant geomagnetic and the subdominant charge-excess mechanisms. Unlike the charge-excess component, which stays constant with the azimuthal direction, the geomagnetic emission varies with the shower direction since it is proportional to the Lorentz force and scales as  $\mathcal{E}_{\text{geo}} \propto qvB \sin \alpha$ , with  $\alpha$  the geomagnetic angle. Hence, to account for the variation of the radio emission with the shower azimuth, we have to separate the geomagnetic and charge-excess contributions at the antenna level and scale the geomagnetic component only. In practice, such a separation can be done using symmetries of the radio signal in the shower plane  $[\mathbf{v} \times \mathbf{B}; \mathbf{v} \times (\mathbf{v} \times \mathbf{B})]$ , which yields [16, 17]

$$\mathcal{E}_{\text{ce}} = \frac{\mathcal{E}_{v \times (v \times B)}}{|\sin \phi_{\text{obs}}|}, \quad (3)$$

$$\mathcal{E}_{\text{geo}} = \mathcal{E}_{v \times B} - \mathcal{E}_{v \times (v \times B)} \frac{\cos \phi_{\text{obs}}}{|\sin \phi_{\text{obs}}|}, \quad (4)$$

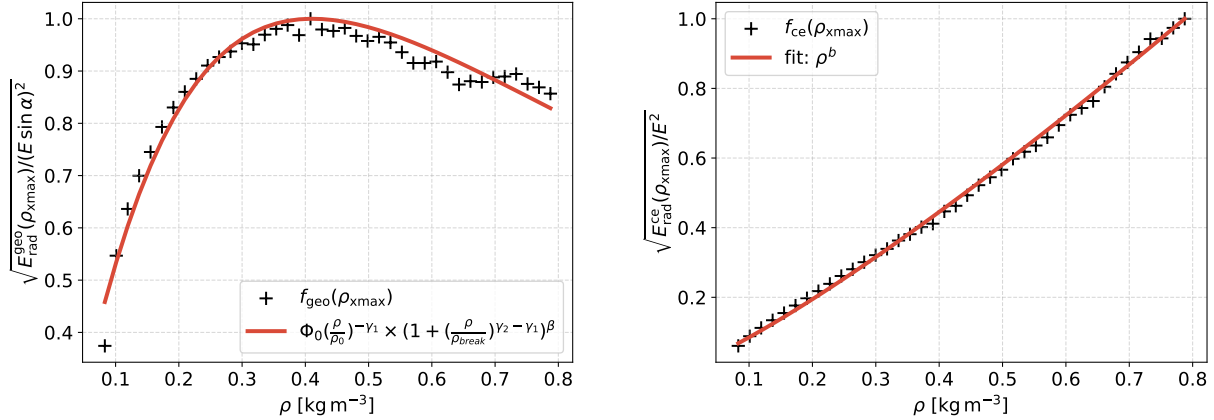


Figure 3: (Left) Average geomagnetic electric field amplitude dependency with air-density (black crosses), from ZHAireS simulations. Results are fitted with a broken power law (red line), using  $\phi_0 = 1010$ ,  $\gamma_1 = -1.0047$ ,  $\gamma_2 = 0.2222$ ,  $\rho_{\text{break}} = 3.5 \times 10^{-4}$ ,  $\beta = 2.5$  and  $\rho_0 = 1.87 \times 10^{-6}$ . (Right) Average charge excess electric field amplitude dependency with air-density from ZHAireS simulations. Results are fitted with a simple power law, using  $b = 1.195$ . Both plots are normalized by their maximal value.

with  $\phi_{\text{obs}}$  is the angle between the antenna position in the shower plane and the  $(\mathbf{v} \times \mathbf{B})$  axis. This equation diverges along the  $v \times B$  axis ( $\phi_{\text{obs}} = 0$ ), but it can be generalized to any antenna position by using the specific case where  $\phi_{\text{obs}} = \pi/2$ , corresponding to antennas along the  $v \times (v \times B)$  axis, and assuming a radial symmetry of the radio signal in the shower plane. The scaling of the radio emission with the geomagnetic angle affects only the  $(v \times B)$  component of the traces and is then given by

$$\mathcal{E}_{v \times B}^t(t, \omega) = -[k_{\text{geo}} \mathcal{E}_{\text{geo}}^r(t, \omega) + \cos \phi_{\text{obs}} \mathcal{E}_{\text{ce}}^r(t, \omega)], \quad (5)$$

where  $k_{\text{geo}} = \sin \alpha_t / \sin \alpha_r$ ,  $\mathcal{E}_{\text{geo}}^r(t, \omega)$  and  $\mathcal{E}_{\text{ce}}^r(t, \omega)$  are the electric field amplitudes related to the geomagnetic and charge-excess emissions for the reference shower, evaluated at an angle  $\omega$  from the shower axis and for an observer angle  $\phi_{\text{obs}}$ .

For a typical magnetic field  $B = 56 \mu\text{T}$ , the charge-excess emission accounts for only  $\sim 10\%$  of the signal amplitude for showers with zenith angle  $\theta = 60^\circ$ , and decreases with increasing zenith angle, becoming almost negligible for showers with zenith angle  $\theta > 80^\circ$  [18]. Hence, for the most inclined showers, assuming a radial symmetry to separate the geomagnetic and charge-excess emissions may rather deteriorate the Radio Morphing accuracy. Consequently, for showers with  $\theta > 70^\circ$  or in the case where the scaling correction factor is small  $|1 - k_{\text{geo}}| < 0.2$  we do not disentangle between the geomagnetic and charge-excess emission and scale directly the  $(v \times B)$  component of the electric field

following

$$\mathcal{E}_{v \times B}^t(t, \omega) = k_{\text{geo}} \mathcal{E}_{v \times B}^r(t, \omega). \quad (6)$$

Similarly to what was done with the energy scaling, we show in the bottom plots of Fig. 2 the  $(v \times B)$  component of the LDF along the  $[\mathbf{v} \times (\mathbf{v} \times \mathbf{B})]$  direction, for a reference and a target shower with a different azimuth angle, before and after the scaling procedure. Here again, we can estimate the efficiency of the method by computing the relative differences in the integral of the two LDF. Much better agreement is found between the two showers, once the scaling procedure has been applied, with  $\delta I/I = -18.19\%$  before the scaling and  $\delta I/I = -4.3\%$  after scaling. The modeling of the charge-excess emission is a major improvement compared to [12] which was assuming a pure geomagnetic emission.

### 3.4. Altitude at $X_{\text{max}}$

As mentioned in Section 3.1, a change in the primary composition or in the shower zenith angle will change the altitude at  $X_{\text{max}}$  since inclined air showers are expected to develop higher in the atmosphere than vertical ones. Such a variation will impact both the refractive index and the air density at  $X_{\text{max}}$ .

The variation of the air refractive index  $n_{\text{air}}$  at  $X_{\text{max}}$  was already modeled in [12]. The refractive index is directly linked to the Cherenkov angle through  $\theta_c = \arccos 1/n_{\text{air}} \beta$ , which yields the characteristic scale of the radio signal amplitude pattern. We can account for

modifications of  $n_{\text{air}}$  by stretching the reference antenna positions by a factor given by the ratio of the Cherenkov angle between the target and the reference shower. We get  $\mathbf{x}^t = k_c \mathbf{x}^r$  with  $k_c = \theta_c^r / \theta_c^t$ . Since the shower energy must be conserved, we also scale the electric field traces with the inverse factor  $\mathcal{E}^t(\mathbf{x}^t, t) = \frac{\mathcal{E}^r(\mathbf{x}^r, t)}{k_c}$ .

Variations in the shower altitude also affect the air density at  $X_{\text{max}}$ . The previous version of Radio Morphing was limited to a narrow zenith-angle range, being valid only for nearly horizontal showers ( $\theta \gtrsim 86^\circ$ ). In the updated version, we account for the dependence of the radio emission on the air density at  $X_{\text{max}}$ , which extends the range of validity to zenith angles between  $60^\circ$  and  $87.1^\circ$ . Following [19], we model this dependency using a set of 11 000 ZHAireS simulations of cosmic-ray showers (with proton or iron primaries) on a star-shape layout, with zenith angles between  $45^\circ$  and  $90^\circ$ , energies between 0.01 EeV and 3.98 EeV and 4 azimuth angles ( $0^\circ, 90^\circ, 180^\circ, 270^\circ$ ). For each air shower, we reconstructed the charge excess and geomagnetic radiation energies  $E_{\text{rad}}^{\text{ce}}$  and  $E_{\text{rad}}^{\text{geo}}$ , by separating each component and integrating their energy fluence following [20, 19]. These energies were then corrected from any dependency on the primary particle energy and on the geomagnetic angle using

$$\tilde{E}_{\text{rad}}^{\text{geo}} = \frac{E_{\text{rad}}^{\text{geo}}}{(\mathcal{E} \times \sin \alpha)^2} \quad \text{and} \quad \tilde{E}_{\text{rad}}^{\text{ce}} = \frac{E_{\text{rad}}^{\text{ce}}}{\mathcal{E}^2}, \quad (7)$$

with  $\mathcal{E}$ , the primary energy and where a correction in  $\mathcal{E}^2$  is applied since the radiation energy scales with the square of the electric field, which itself is proportional to the primary energy. The residual variations of  $\tilde{E}_{\text{rad}}^{\text{geo}}$  and  $\tilde{E}_{\text{rad}}^{\text{ce}}$  should thus stem from density effects only. Finally, since the electric field scales with the square root of the radiation energy, the geomagnetic and charge-excess electric field dependency with air density at  $X_{\text{max}}$  can be derived from  $\sqrt{\tilde{E}_{\text{rad}}^{\text{geo}}(\rho_{X_{\text{max}}})}$  and  $\sqrt{\tilde{E}_{\text{rad}}^{\text{ce}}(\rho_{X_{\text{max}}})}$ . Assuming the Linsley atmospheric model, we can fit these dependencies with two functions that we denote  $f_{\text{geo}}(\rho_{X_{\text{max}}})$  and  $f_{\text{ce}}(\rho_{X_{\text{max}}})$  respectively.

In Fig. 3, we show the geomagnetic and charge-excess emission dependency with air density at  $X_{\text{max}}$ . The right-hand panel shows that the charge-excess amplitude increases almost linearly with the air density, as also shown in [20]. Indeed, a higher density provides more air atoms that can be ionized by the shower, leading to a larger build-up of negative charges, resulting in a stronger charge-excess emission. The left-hand panel shows that the geomagnetic emission first increases and then decreases when decreasing the air density at  $X_{\text{max}}$ ,

i.e., for more inclined showers. When the shower inclination increases, charged particles can reach a larger drift velocity which initially results in a stronger transverse current and a larger geomagnetic emission [9]. Yet, if the shower is too inclined and the magnetic field is strong enough, the shower lateral extent at  $X_{\text{max}}$  becomes so large that the radio emission becomes incoherent, causing the drop observed for the lowest air densities as characterized in [21]. As a result, the charge-excess emission was fitted using a simple power law, while the geomagnetic emission was fitted using a broken power-law.

### 3.5. Shower-to-shower fluctuations

Due to the probabilistic nature of interactions occurring in air-showers, the radio-emission from various showers induced by primary particles with identical mass composition, energy, and arrival direction, presents some differences that we refer to as shower-to-shower fluctuations. These fluctuations are intrinsically modeled by Monte-Carlo simulations for which hadronic interactions are evaluated in a probabilistic way. However, Radio Morphing uses only a small sample of reference showers; hence, hadronic interactions are not recomputed when generating new simulations. This allows one to considerably reduce the computation time but requires further implementation of shower-to-shower fluctuations that are consistent with the simulation data. Another improvement of this new Radio Morphing version is the implementation of shower-to-shower fluctuations, which can now be enabled by the user. The modeling of these effects relies on parametrizations of: (1)  $X_{\text{max}}$  fluctuations and (2) the fluctuations of the number of particles in the shower.

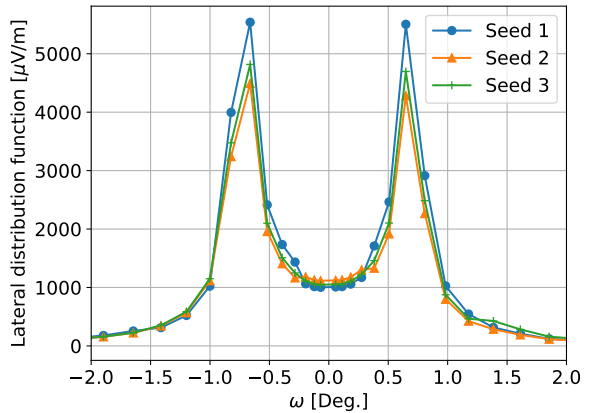


Figure 4: Example of shower-to-shower fluctuations. LDFs generated with Radio Morphing for three showers with the same input parameters ( $E = 3.98 \text{ EeV}$ ,  $\theta = 75^\circ$ ,  $\varphi = 180^\circ$ ) but different random seed.

In addition to the parametrization of the mean  $X_{\max}$  grammage discussed in Section 3.1, it is also possible to parameterize the  $X_{\max}$  root mean square using a function of the form  $\sigma_{X_{\max}} = a + b/E^c$ . From a set of 11 000 ZHAireS simulations this yields  $a = 66.5 \text{ g.cm}^{-2}$ ,  $b = 2.84 \text{ g.cm}^{-2} \cdot (\text{E}[\text{TeV}])^c$ ,  $c = 0.48$  for proton primaries and  $a = 20.9 \text{ g.cm}^{-2}$ ,  $b = 3.67 \text{ g.cm}^{-2} \cdot (\text{E}[\text{TeV}])^c$ ,  $c = 0.21$  for iron primaries. Hence, when shower-to-shower fluctuations are enabled by the user, the Radio Morphing generates a  $X_{\max}$  grammage from a Gaussian distribution, using  $\langle X_{\max} \rangle$  and  $\sigma_{X_{\max}}$  as input parameters.

We also studied the fluctuation of the number of particles in air-showers using ZHAireS simulations: we computed the number of positrons and electrons,  $N_{e^+e^-}$  that cross a plane perpendicular to the shower axis at  $X_{\max}$  for showers with various arrival directions but fixed energy. We find fluctuations of roughly 10% independently of the zenith angle and of the primary particle energy. In Radio Morphing, we can model the fluctuations of  $N_{e^+e^-}$  by introducing fluctuations of the target shower primary particle energy, since both quantities scale linearly. In practice, this is done by randomly drawing a shower energy in a Gaussian distribution of 10% sigma value around the target energy  $\mathcal{E}_t$ , specified by the user. Shower-to-shower fluctuations of  $X_{\max}$  and  $N_{e^+e^-}$  are illustrated in the left-hand panel of Fig. 4, where we show the LDF of three showers simulated with Radio Morphing with the exact same input parameters. It can be seen that the fluctuations do not significantly affect the LDF shape but can change the electric field amplitude at the antennas' level by roughly 10%.

### 3.6. Interpolation and extrapolation

Once the scaling procedure is completed, we perform a 2D interpolation of the radio signal in the scaled plane of antennas illustrated in Fig. 1, to infer the radio emission at any desired position within the plane. For this purpose, we rely on the method presented in [22] where the traces are decomposed into a phase and amplitude in Fourier space which are then interpolated independently using the closest neighbor antennas. When considering antennas away from the Cherenkov angle, the method provides relative differences with ZHAireS simulations of only a few percent on both the peak-to-peak amplitude and integrated pulse, combined with a timing error of less than 5 nanoseconds. This is a major improvement compared to the initial version of the Radio Morphing implementation ([12]).

Eventually, to evaluate the radio emission at various longitudinal distances, the 2D interpolation is coupled

with a 3D extrapolation, as illustrated in Fig. 1. In practice, for any target antenna at a distance  $d_{\text{ant}}^{X_{\max}}$  from  $X_{\max}$ , with an angular deviation from the shower axis  $\omega$  and an observer angle  $\phi_{\text{obs}}$ , we first perform a 2D interpolation within the scaled plane for the antenna with the same  $(\omega, \phi_{\text{obs}})$  angles. The radio emission at the target antenna is then inferred from the scaled one by performing an extrapolation that accounts for propagation effects (propagation of the blue dashed line from the red scaled plane in Fig. 1 to the extrapolated signal on ground). This modeling assumes that the radio emission amplitude pattern in the shower plane, in the  $(\omega, \phi_{\text{obs}})$  representation, is invariant by translation along the shower axis.

The correction for the propagation effects assumes a point-link emission at  $X_{\max}$ , so that the radio emission electric field amplitude decreases linearly with the distance to  $X_{\max}$ . For fixed  $(\omega, \phi_{\text{obs}})$  angles, considering a scaled antenna at a distance  $d_{\text{scaled}}$  from  $X_{\max}$  and a target antenna at a distance  $d_{\text{target}}$ , our correction yields

$$\mathcal{E}_{\text{target}}(\omega, \phi_{\text{obs}}) = \frac{d_{\text{scaled}}}{d_{\text{target}}} \mathcal{E}_{\text{scaled}}(\omega, \phi_{\text{obs}}). \quad (8)$$

A second correction consists in accounting for the difference in the integrated refractive index between the scaled and the extrapolated signals. Indeed, antennas at different longitudinal distances will see a different integrated refractive index from  $X_{\max}$  to their position. This effect is corrected by applying a stretching factor to the antenna positions and the traces  $k_{\text{stretch}} = \theta_c^{\text{int}}/6_{\text{c}}^{\text{scaled}} = (\arccos 1/\bar{n}_{\text{int}})/(\arccos 1/\bar{n}_{\text{scaled}})$ , similarly to what was done for the modeling of the air density effects in the scaling with the zenith angle (Section 3.4).

## 4. Radio Morphing Performances

The Radio Morphing performances on the radio signal amplitude, timing, and frequency spectrum are evaluated by comparing Radio Morphing outputs to ZHAireS simulations run with the same input parameters (mass composition, primary energy, arrival direction, and antenna positions). For this purpose, we generated with Radio Morphing  $\sim 4500$  proton or iron showers in the energy range  $E = [0.2 - 3.98] \text{ EeV}$ , zenith angles between  $\theta = [63^\circ - 87.1^\circ]$ , and for 3 azimuth angles  $\varphi = [0^\circ, 90^\circ, 180^\circ]$ .

### 4.1. Amplitude results

For each Radio Morphing test simulation, the radio signal was generated at 176 antenna positions located

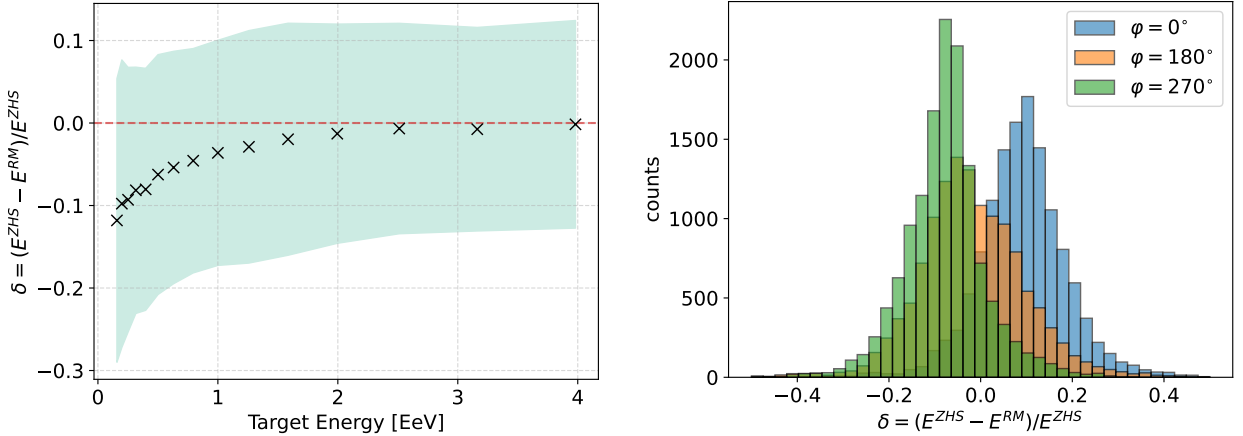


Figure 5: (Left) Relative differences  $\delta$  on the electric field peak amplitude between ZHAireS and Radio Morphing simulations as a function of the shower energy. Crosses show the mean value of  $\delta$  while the shaded area corresponds to its standard deviation. (Right) Distribution of  $\delta$  at the antenna level for showers with three different azimuth angles.

at an altitude of 1086 meters above sea level, and compared to the same outputs produced with ZHAireS simulations. We then quantified the efficiency of our method by evaluating the relative differences in amplitude of the electric field amplitude between ZHAireS and Radio Morphing simulations using

$$\delta = \left\langle \frac{E^{ZHS}(t) - E^{RM}(t)}{E^{ZHS}(t)} \right\rangle_{>0.2E_{ZHS}^{\text{peak}}}, \quad (9)$$

where the brackets denote an average over time samples with amplitudes exceeding 20% of the ZHAireS peak value. This metric was preferred over a simple comparison of peak amplitudes, as it remains valid even for filtered signals, where the power is distributed over several samples. We also note that for each antenna, the dominant channel is used to evaluate the value of  $\delta$ . Using this metric, the mean value of  $\delta$  over different signals quantifies the accuracy of our method (bias), while the standard deviation of  $\delta$  evaluates the precision of Radio Morphing.

In the left-hand panel of Fig. 5, we show the mean (crosses) and standard deviation (blue shaded area) of the relative differences  $\delta$  in the total peak amplitude at the antenna level, between the ZHAireS and Radio Morphing simulations, as a function of the target shower energy. We get mean relative differences close to  $\delta = 0\%$  and standard deviations of  $\sim \delta = 10\%$  for the most energetic showers, with energies above 1 EeV, while both the precision and accuracy of Radio Morphing decrease for the lowest-energy showers. This loss of efficiency at low energy comes from two main effects. First, as mentioned in Section 2, our reference showers were run

with a primary energy of  $\mathcal{E}_r = 3.98$  EeV, so the lowest primary energies in Fig. 5 are also the farthest from the reference one. Second, higher fluctuations of the radio emission are typically expected for low-energy showers in Monte Carlo simulations because of thinning effects.

The right-hand panel of Fig. 5 shows the distribution of  $\delta$  for the three azimuth angles tested in our simulations. We observe a slight azimuth-dependent bias, as the distributions are not exactly centered on  $\delta = 0$ , the largest deviations being observed for  $\varphi = 0^\circ$ . This effect is still under investigation, but is probably related to the fact that showers with smaller geomagnetic angles, typically for  $\varphi = 0^\circ$  at the Dunhuang location, experience less coherence loss and therefore produce stronger radio emission after correction from the  $\sin \alpha$  effect [21, 23]. However, our scaling of radio emission with the zenith angle shown in Fig. 3, which incorporates the coherence loss effects, relies on an average fit for all azimuth angles and therefore does not account for the azimuth-dependent effect. This will be corrected in further Radio Morphing implementations.

In Fig. 6, we show the mean (crosses) and standard deviation (shaded area) of  $\delta$  as a function of the antenna angular deviation from the shower axis,  $\omega$ . The mean relative differences between ZHAireS and Radio Morphing remain roughly constant across antenna positions, which indicates that there is no significant bias related to the antenna positions. The standard deviations are also constant at large  $\omega$ , but a significant increase appears around  $\omega = 0.6^\circ$ , i.e., near the Cherenkov angle. This effect is mainly due to the reduced performance of the radio signal interpolation at the Cherenkov angle, where

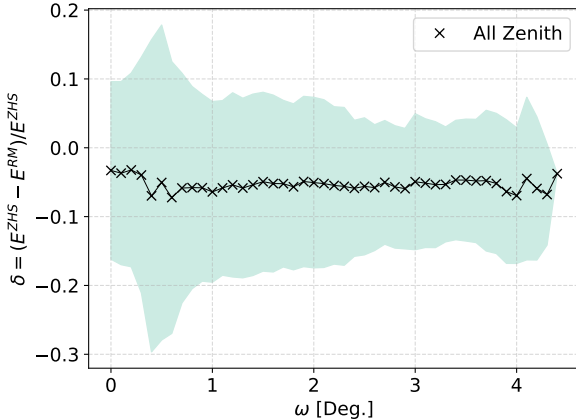


Figure 6: Mean (crosses) and standard deviation (shaded area) of the relative differences  $\delta$  on the electric field peak amplitude, between ZHAireS and Radio Morphing simulations, as a function of the radio antenna positions. The  $\omega$  angle corresponds to the angular deviation of the antennas from the shower axis.

the spatial variations of the radio signal amplitude are stronger. This feature could be improved by using reference ZHAireS simulations with an even denser antenna grid close to the Cherenkov angle.

In Fig. 7 we show the mean (left-hand panel) and standard deviations (right-hand panel) of  $\delta$  as a function of the target shower zenith angle. For the average values of  $\delta$  we distinguish between the case where the target zenith angle is the same as that of our reference showers (blue crosses) and the cases where both quantities are different (orange crosses). For most zenith angles, Radio Morphing provides mean relative differences in the peak amplitude of less than 5%, evidencing a minor bias in our simulations. Larger deviations are observed only for showers with target zenith angles that are relatively far from any reference zenith angle in our library. Typically for  $\theta = 72^\circ$ , while the closest showers have either  $\theta^{\text{ref}} = 69.8^\circ$  or  $\theta^{\text{ref}} = 74.8^\circ$ . This highlights that the efficiency of Radio Morphing depends on the proximity of the target showers to the reference ones, but it also indicates that its performance could be improved by adding more reference showers. The right-hand panel of Fig. 7 shows that Radio Morphing achieves standard deviations of the peak-amplitude error below 17% over the full zenith-angle range, and even below 12% for the most vertical and the most inclined showers. This behavior can be understood as follows: vertical showers are generally easier to model, since their radio emission varies less steeply with zenith angle and their footprints are more symmetric. At large zenith angles, the improved precision originates from the higher density

of reference showers in our library, which enhances the interpolation accuracy of the Radio Morphing method.

#### 4.2. Filtered results

To further assess the performances of Radio Morphing, we evaluated its precision after applying frequency filtering and different trigger thresholds. Figure 8 shows the standard deviation of  $\delta$  as a function of zenith angle for unfiltered traces, traces filtered in the [50–200] MHz band, and traces in the [30–80] MHz band. Assuming that the typical stationary background noise has a standard deviation of  $22 \mu\text{V/m}$  [24], a trigger threshold of  $60 \mu\text{V/m}$  ( $3\sigma$ ) was applied for the results shown in the left-hand panel, and  $110 \mu\text{V/m}$  ( $5\sigma$ ) for the right-hand panel. To ensure a consistent comparison, all trigger thresholds were defined with respect to the signal filtered in the [30–80] MHz band. We find standard deviations below 15% independently of the frequency band, trigger threshold, and zenith angle. We can also observe some fluctuations which are once again related to target zenith angles relatively far from our reference showers (typically for  $\theta = 72^\circ$  and  $\theta = 81.3^\circ$ ). We further notice that the performances in the GRAND frequency band ([50–200] MHz) are not necessarily better than the full band results. This effect seems to be linked mainly to low-amplitude signals, as for a trigger threshold of  $110 \mu\text{V/m}$  (right-hand plot) results in the GRAND frequency band get better than in the full band results for vertical showers only. Eventually, we observe that Radio Morphing reaches its best efficiency in the [30–80] MHz band with most standard deviations being even below 10%. This highlights that Radio Morphing is more efficient at low frequency. This can be expected as high frequency signals are located close to Cherenkov cone where the spatial variability of the radio emission is large, which makes the interpolation less efficient. Overall, these results show that Radio Morphing can accurately reproduce the radio signal from cosmic ray-induced air showers, with relative differences with ZHAireS simulations within the range of calibration uncertainties expected for radio experiments (typically of 20% [1]).

#### 4.3. Timing

We also evaluated Radio Morphing performances on the peak-time reconstruction. A precise timing resolution is essential for the angular reconstruction of the arrival direction of the shower. For this, we evaluated the absolute peak-time difference, at the antenna level, between ZHAireS and Radio Morphing simulations. In the left-hand panel of Fig. 9, we show the distribution

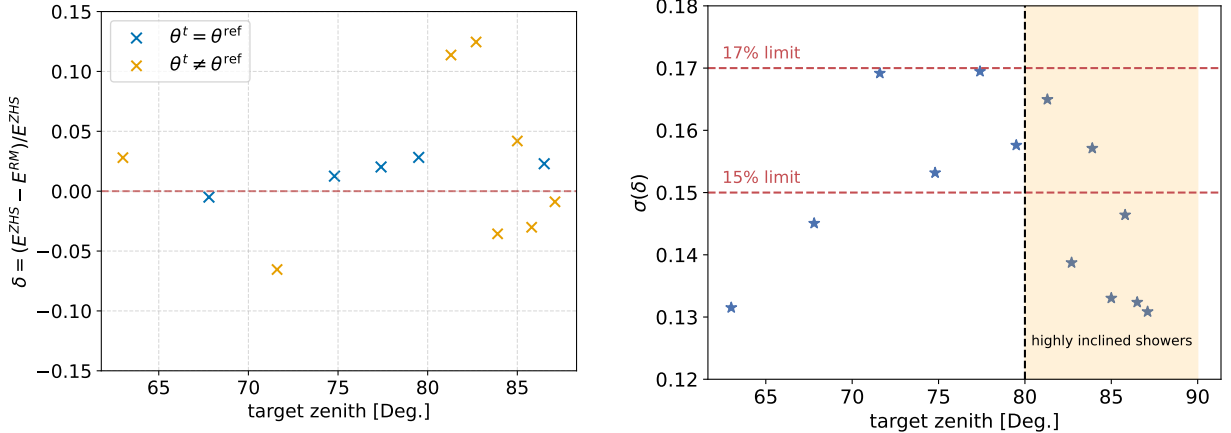


Figure 7: Mean (left-hand panel) and standard deviation (right-hand panel) of the relative differences  $\delta$  on the electric field peak amplitude, between ZHAireS and Radio Morphing simulations, as a function of the shower zenith angle, without any trigger threshold.

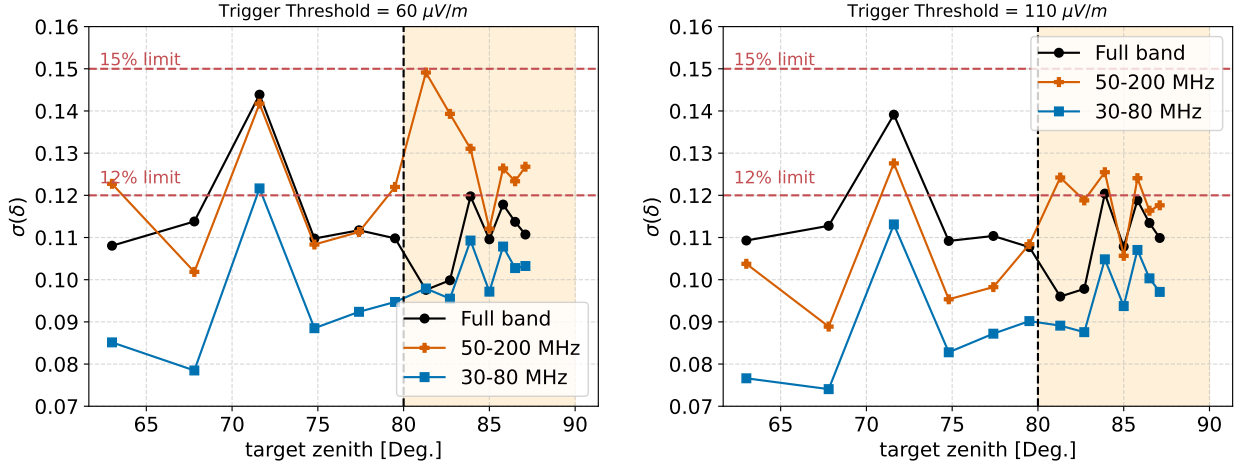


Figure 8: Standard deviations of the relative differences  $\delta$  on the electric field peak amplitude, between ZHAireS and Radio Morphing simulations, as a function of the shower zenith angle. The results are shown for three different frequency bands: full band (black line), [50 – 200] MHz (orange line) and [30 – 80] MHz (blue line). The left-hand panel corresponds to a  $3\sigma$  trigger threshold ( $60 \mu\text{V/m}$ ), while the right-hand plot is for a  $5\sigma$  trigger threshold ( $110 \mu\text{V/m}$ ). The shaded area delimits the most inclined showers ( $\theta > 80^\circ$ ).

of the peak-time delay between Radio Morphing and ZHAireS simulations. For more than 99% of antennas we get a time difference  $\Delta t$  within  $\pm 5\text{ns}$ , i.e., below the typical timing resolution of most radio experiments. This performance is allowed by the new interpolation method used in this version of Radio Morphing [12] and is a major improvement compared to the version of [19].

#### 4.4. Computation time

Eventually, we evaluated the CPU time of Radio Morphing simulations, since the primary objective of the tool is to simulate air shower radio signals for future large-scale radio experiments such as GRAND or the

Pierre Auger Observatory. In the right-hand panel of Fig. 9, we show the mean CPU time of Radio Morphing as a function of the shower zenith angle from the set of 4500 showers generated with Radio Morphing to test its performances. Each simulation corresponds to a thinning of  $10^{-5}$  and was run for 176 antennas with a primary energy between  $10^{17} \text{ eV}$  and  $4 \cdot 10^{18} \text{ eV}$ . It can be seen that the computation time increases with the zenith angle, which is expected, as more reference planes are used for inclined showers. Still, Radio Morphing provides a computation time of only a few tens of seconds, independently of the shower zenith angle and primary energy. For a quantitative comparison, simulations with

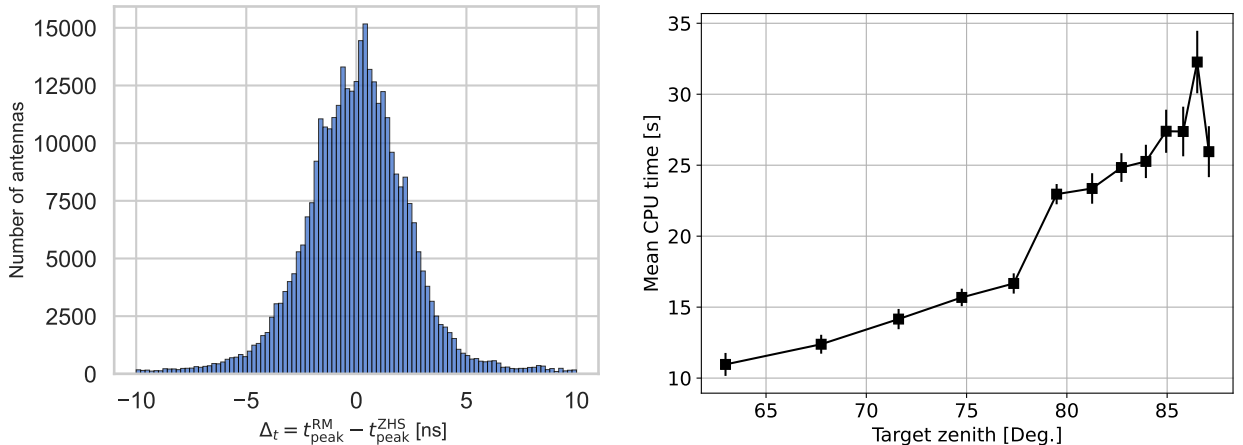


Figure 9: (Left) Peak-time delay at the antenna level between Radio Morphing and ZHAireS simulations. (Right) Mean CPU time (square) and standard deviation (error bars) of Radio Morphing simulations as a function of the shower zenith angle. For each shower, the radio emission was simulated at 176 antenna positions with a thinning of  $10^{-5}$ .

the same thinning, primary energy, and number of antennas, run with ZHAireS or CoREAS, are generally expected to take  $\sim 1 - 2$  days of CPU time (with AMD EPYC 7302 16-Core Processor) for  $\theta = 60^\circ$  and around 1 week for  $\theta = 85^\circ$ . This leads to an improvement of more than 4 orders of magnitude, making Radio Morphing a suitable tool to run a massive number of simulations in a short amount of time, in preparation for future large-scale radio detectors.

## 5. Conclusion

We presented the latest version of Radio Morphing, a semi-analytical method that allows for a fast computation of any cosmic-ray induced air shower with zenith angle  $\theta > 60^\circ$ , at any desired position in space, from the simulation data of a few reference ZHAireS showers at given positions. This new version now incorporates shower-to-shower fluctuations, refined scaling laws, interpolation method, and modeling of charge-excess emission. Radio Morphing performances were evaluated by comparison to ZHAireS simulations ran for the same parameters. For most zenith angles, we find mean relative differences in the full band peak amplitude around 5%, indicating only a minor bias of the method, mainly for low-energy showers with an azimuthal direction close to the magnetic North. The corresponding standard deviations on raw traces were evaluated to be below 17% independently of the zenith angle, i.e., below the calibration error reached by current radio detectors. The standard deviations were even reduced to 15% when applying a  $3\sigma$  trigger threshold

and below  $\sim 10\%$  when working in the  $[30 - 80]$  MHz band. These performances were coupled with a timing accuracy of less than 5 ns and a time computation reduced by more than four orders of magnitude compared to standard Monte Carlo simulations with primary energy above  $10^{17}$  eV. This makes Radio Morphing a powerful and accurate tool for simulating a huge number of air shower simulations in the view of future large-scale radio detectors such as GRAND, SKA, or the radio upgrade of the Pierre Auger Observatory. Further improvements would include the correction of the bias with the shower azimuth angle, an implementation of radio emission scaling with the Earth's magnetic field and the incorporation of other primaries such as neutrinos. Radio Morphing open source code is written in python and now publicly available at <https://github.com/simonchiche/RadioMorphing>.

## Acknowledgments

We thank the CC-IN2P3 Computing Centre (Lyon/Villeurbanne – France), partnership between CNRS/IN2P3 and CEA/DSM/Irfu, for the computing ressources. We thank the GRAND collaborators and in particular Kumiko Kotera for useful discussions and comments.

## References

[1] J. Álvarez-Muñiz, et al., The Giant Radio Array for Neutrino Detection (GRAND): Science and design, *Science China Physics, Mechanics, and Astronomy* 63 (1) (2020) 219501. [arXiv:1810.09994](https://arxiv.org/abs/1810.09994), doi:10.1007/s11433-018-9385-7.

[2] D. Southall, et al., Design and initial performance of the prototype for the beacon instrument for detection of ultrahigh energy particles, *Nuclear Instruments and Methods in Physics Research Section A: Accelerators, Spectrometers, Detectors and Associated Equipment* 1048 (2023) 167889. doi:<https://doi.org/10.1016/j.nima.2022.167889>. URL <https://www.sciencedirect.com/science/article/pii/S0168900222011810>

[3] A. Corstanje, S. Bouma, S. Buitink, M. Desmet, J. R. Hörandel, T. Huege, P. Laub, K. Mulrey, A. Nelles, O. Scholten, K. Terveer, S. Thoudam, K. Watanabe, LOFAR-style reconstruction of cosmic-ray air showers with SKA-Low, *Phys. Rev. D* 112 (2) (2025) 023017. [arXiv:2504.16873](https://arxiv.org/abs/2504.16873), doi:10.1103/18mt-994v.

[4] T. Huege, Pierre Auger Collaboration, Radio detection of cosmic rays with the Auger Engineering Radio Array, in: European Physical Journal Web of Conferences, Vol. 210 of European Physical Journal Web of Conferences, 2019, p. 05011. [arXiv:1905.04986](https://arxiv.org/abs/1905.04986), doi:10.1051/epjconf/201921005011.

[5] S. J. Sciutto, <http://aires.fisica.unlp.edu.ar/zaires> (2021).

[6] J. Alvarez-Muñiz, W. R. Carvalho, E. Zas, Monte Carlo simulations of radio pulses in atmospheric showers using ZHAireS, *Astroparticle Physics* 35 (6) (2012) 325–341. [arXiv:1107.1189](https://arxiv.org/abs/1107.1189), doi:10.1016/j.astropartphys.2011.10.005.

[7] D. Heck, J. Knapp, J. N. Capdevielle, G. Schatz, T. Thouw, CORSIKA: a Monte Carlo code to simulate extensive air showers., 1998.

[8] T. Huege, M. Ludwig, C. W. James, Simulating radio emission from air showers with CoREAS, in: R. Lahmann, T. Eberl, K. Graf, C. James, T. Huege, T. Karg, R. Nahnhauer (Eds.), 5th International Workshop on Acoustic and Radio EEV Neutrino Detection Activities: Arena 2012, Vol. 1535 of American Institute of Physics Conference Series, 2013, pp. 128–132. [arXiv:1301.2132](https://arxiv.org/abs/1301.2132), doi:10.1063/1.4807534.

[9] O. Scholten, K. Werner, F. Rusydi, A macroscopic description of coherent geo-magnetic radiation from cosmic-ray air showers, *Astroparticle Physics* 29 (2) (2008) 94–103. [arXiv:0709.2872](https://arxiv.org/abs/0709.2872), doi:10.1016/j.astropartphys.2007.11.012.

[10] O. Scholten, T. Trinh, K. de Vries, B. Hare, Analytic calculation of radio emission from parametrized extensive air showers: A tool to extract shower parameters, *Phys. Rev. D* 97 (2) (2018) 023005. [arXiv:1711.10164](https://arxiv.org/abs/1711.10164), doi:10.1103/PhysRevD.97.023005.

[11] M. Desmet, K. Watanabe, T. Huege, S. Buitink, SMIET: Fast and accurate synthesis of radio pulses from extensive air shower using simulated templates, *arXiv e-prints* (2025) [arXiv:2505.10459](https://arxiv.org/abs/2505.10459), doi:10.48550/arXiv.2505.10459.

[12] A. Zilles, et al., Radio Morphing: towards a fast computation of the radio signal from air showers, *Astroparticle Physics* 114 (2020) 10–21. doi:10.1016/j.astropartphys.2019.06.001.

[13] D. Góra, R. Engel, D. Heck, P. Homola, H. Klages, J. Pełka, M. Risse, B. Wilczyńska, H. Wilczyński, Universal lateral distribution of energy deposit in air showers and its application to shower reconstruction, *Astroparticle Physics* 24 (6) (2006) 484–494. [arXiv:astro-ph/0505371](https://arxiv.org/abs/astro-ph/0505371), doi:10.1016/j.astropartphys.2005.09.007.

[14] S. J. Sciutto, Aires: A system for air shower simulations (1999). doi:10.48550/ARXIV.ASTRO-PH/9911331. URL <https://arxiv.org/abs/astro-ph/9911331>

[15] R. Engel, D. Heck, T. Pierog, Extensive air showers and hadronic interactions at high energy, *Annual Review of Nuclear and Particle Science* 61 (1) (2011) 467–489. [arXiv:https://doi.org/10.1146/annurev.nucl.012809.104544](https://arxiv.org/abs/https://doi.org/10.1146/annurev.nucl.012809.104544), doi:10.1146/annurev.nucl.012809.104544. URL <https://doi.org/10.1146/annurev.nucl.012809.104544>

[16] T. Huege, F. Schlüter, L. Brenk, Symmetrizing the signal distribution of radio emission from inclined air showers, in: 36th International Cosmic Ray Conference (ICRC2019), Vol. 36 of International Cosmic Ray Conference, 2019, p. 294. [arXiv:1908.07840](https://arxiv.org/abs/1908.07840), doi:10.22323/1.358.0294.

[17] Pierre Auger Collaboration, Measurement of the Radiation Energy in the Radio Signal of Extensive Air Showers as a Universal Estimator of Cosmic-Ray Energy, *Phys. Rev. Lett.* 116 (24) (2016) 241101. [arXiv:1605.02564](https://arxiv.org/abs/1605.02564), doi:10.1103/PhysRevLett.116.241101.

[18] S. Chiche, K. Kotera, O. Martineau-Huynh, M. Tueros, K. D. de Vries, Polarisation signatures in radio for inclined cosmic-ray induced air-shower identification, *Astroparticle Physics* 139 (2022) 102696. [arXiv:2202.06846](https://arxiv.org/abs/2202.06846), doi:10.1016/j.astropartphys.2022.102696.

[19] S. Chiche, O. Martineau-Huynh, K. Kotera, M. Tueros, K. D. de Vries, Radio-Morphing: a fast, efficient and accurate tool to compute the radio signals from air-showers, in: 37th International Cosmic Ray Conference, 2022, p. 194. [arXiv:2202.05886](https://arxiv.org/abs/2202.05886), doi:10.22323/1.395.0194.

[20] C. Glaser, M. Erdmann, J. R. Hörandel, T. Huege, J. Schulz, Simulation of radiation energy release in air showers, *J. Cosmology Astropart. Phys.* 2016 (9) (2016) 024. [arXiv:1606.01641](https://arxiv.org/abs/1606.01641), doi:10.1088/1475-7516/2016/09/024.

[21] S. Chiche, C. Zhang, F. Schlüter, K. Kotera, T. Huege, K. D. de Vries, M. Tueros, M. Guelfand, Loss of Coherence and Change in Emission Physics for Radio Emission from Very Inclined Cosmic-Ray Air Showers, *Phys. Rev. Lett.* 132 (23) (2024) 231001. [arXiv:2404.14541](https://arxiv.org/abs/2404.14541), doi:10.1103/PhysRevLett.132.231001.

[22] M. Tueros, A. Zilles, Synthesis of radio signals from extensive air showers using previously computed microscopic simulations, *Journal of Instrumentation* 16 (2) (2021) P02031. [arXiv:2008.06454](https://arxiv.org/abs/2008.06454), doi:10.1088/1748-0221/16/02/P02031.

[23] J. Ammerman-Yebra, J. Alvarez-Muñiz, E. Zas, Density and magnetic field strength dependence of radio pulses induced by energetic air showers, *J. Cosmology Astropart. Phys.* 2023 (8) (2023) 015. [arXiv:2305.11668](https://arxiv.org/abs/2305.11668), doi:10.1088/1475-7516/2023/08/015.

[24] V. Decoene, N. Renault-Tinacci, O. Martineau-Huynh, D. Charrier, K. Kotera, S. Le Coz, V. Niess, M. Tueros, A. Zilles, Radio-detection of neutrino-induced air showers: The influence of topography, *Nuclear Instruments and Methods in Physics Research A* 986 (2021) 164803. [arXiv:1903.10466](https://arxiv.org/abs/1903.10466), doi:10.1016/j.nima.2020.164803.